New Phytologist

Research

Dynamic subcellular translocation of V-type H^+-ATPase is essential for biomineralization of the diatom silica cell wall

Daniel P. Yee, Mark Hildebrand*† and Martin Tresguerres*

Scripps Institution of Oceanography, University of California San Diego, 9500 Gilman Drive, La Jolla, CA 92093, USA

Author for correspondence:
Martin Tresguerres
Tel: +1 858 534 5895
Email: mtresguerres@ucsd.edu

Received: *11 September 2019*
Accepted: *4 November 2019*

New Phytologist (2019)
doi: 10.1111/nph.16329

Key words: biosilica, membrane acidification, protein trafficking, proton pump, silica biomineralization, vacuolar H^+-ATPase.

Summary

- Diatom cell walls, called frustules, are main sources of biogenic silica in the ocean and their intricate morphology is an inspiration for nanoengineering. Here we show dynamic aspects of frustule biosynthesis involving acidification of the silica deposition vesicle (SDV) by V-type H^+ ATPase (VHA).
- Transgenic *Thalassiosira pseudonana* expressing the VHA B subunit tagged with enhanced green fluorescent protein (VHA_B-eGFP) enabled subcellular protein localization in live cells.
- In exponentially growing cultures, VHA_B-eGFP was present in various subcellular localizations including the cytoplasm, SDVs and vacuoles. We studied the role of VHA during frustule biosynthesis in synchronized cell cultures of *T. pseudonana*. During the making of new biosilica components, VHA_B-eGFP first localized in the girdle band SDVs, and subsequently in valve SDVs. In single cell time-lapse imaging experiments, VHA_B-eGFP localization in SDVs precluded accumulation of the acidotropic silica biomineralization marker PDMPO. Furthermore, pharmacological VHA inhibition prevented PDMPO accumulation in the SDV, frustule biosynthesis and cell division, as well as insertion of the silicalemma-associated protein SAP1 into the SDVs. Finally, partial inhibition of VHA activity affected the nanoscale morphology of the valve.
- Altogether, these results indicate that VHA is essential for frustule biosynthesis by acidifying the SDVs and regulating the insertion of other structural proteins into the SDV.

Introduction

Diatoms are a diverse group of eukaryotic phytoplankton found in marine and freshwater ecosystems worldwide, and are responsible for up to 20% of the primary production on the planet (Field *et al.*, 1998). Unique for having a silica cell wall called the frustule, diatoms are the major source of biogenic silica in the ocean and play central roles in oceanic biogeochemical cycling and marine food webs (Falkowski *et al.*, 1998; Yool & Tyrrell, 2003; Falkowski *et al.*, 2004). The diatom frustule consists of an epitheca and hypotheca that assemble together, similar to a Petri dish (Fig. 1) (Pickett-Heaps *et al.*, 1990). Each half comprises a valve on top and a series of concentric ring-shaped girdle bands on the sides that enable cell elongation. Frustules are synthetized in intracellular compartments called silica deposition vesicles (SDVs), which are defined by a membrane called the silicalemma (Drum & Pankratz, 1964; Volcani & Li, 1984). After cytokinesis, a valve is synthesized in each sibling protoplast within an individual SDV close to the cleavage furrow. After valve exocytosis, each girdle band is synthesized in an individual SDV close to the lateral sides of the cell. Silica biomineralization is aided by long-chain polyamines (Poulsen & Kröger, 2004) and proteins located inside SDVs or embedded within the silicalemma, including silicanin-1 (Sin1) (Kotzsch *et al.*, 2017) and silicalemma-associated proteins (SAPs) (Tesson *et al.*, 2017), which induce silica polymerization and guide the detailed nanoscale pattern formation of the frustule (Hildebrand *et al.*, 2018); silaffins (Kröger *et al.*, 1999) have also been shown to aid in this process but have not yet been targeted to the SDV.

The SDV is speculated to originate from the Golgi apparatus (Pickett-Heaps *et al.*, 1990) and to expand by the fusing of spherical vesicles to the silicalemma (Schmid & Schulz, 1979). A predicted acidic pH of *c.* 5 inside the SDV (Vrieling *et al.*, 1999; Herve *et al.*, 2012) is presumed to slow the polymerization of silicic acid in order to prevent uncontrolled silica deposition and allow for proper morphogenesis of the frustule (Iler, 1979). This degree of acidification suggested the involvement of the V-type H^+-ATPase (VHA) (Gordon & Drum, 1994; Hildebrand *et al.*, 2018), an evolutionary conserved multi-subunit protein complex that uses the energy from ATP hydrolysis to transport H^+ across biological membranes of eukaryotic cells (Nishi & Forgac, 2002; Forgac, 2007). VHA is a holoenzyme that consists of a membrane-bound V_0-domain composed of subunits a, d, e, c, c′, c″, and a cytosolic V_1-domain composed of subunits A–H (Sze *et al.*,

*These authors contributed equally to this work.
†This article is dedicated in memory of Dr Mark Hildebrand (1958–2018), who devoted his life to advancing the biotechnological applications and elucidating the beauty and mystery of diatom cell biology.

© 2019 The Authors
New Phytologist © 2019 New Phytologist Trust

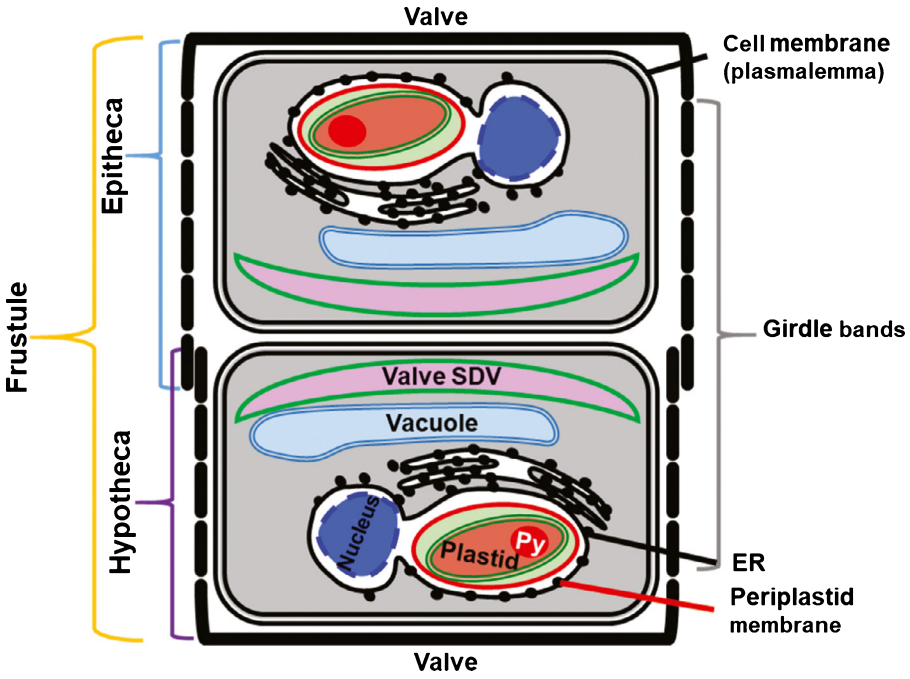


Fig. 1 Diagram of a centric diatom undergoing cell division. The frustule is composed of a hypotheca and overlapping epitheca which encapsulates the cell membrane and all other intracellular compartments. Each theca is composed of a valve and concentric rings of girdle bands. During the M phase following cytokinesis, two valves are synthesized within silica deposition vesicles (SDVs) of two daughter cells and separate the cells when exocytosed. Py, the pyrenoid; ER, endoplasmic reticulum.

1992, 2002; Kluge *et al.*, 2003; Xiao *et al.*, 2008; Bussard & Lopez, 2014; Tresguerres, 2016). The V_0-domain forms a proteolipid ring through membranes, and the V_1-domain hydrolyzes ATP to provide the driving force to move H^+ against its electrochemical gradient (Kawasaki-Nishi *et al.*, 2003).

V-type H^+-ATPase was first proposed in diatom silicification in the role of acidifying clathrin-coated silica transport vesicles to prevent premature hardening of silica before delivery to SDV (Gordon & Drum, 1994). Later, a functional study using pharmacological VHA inhibitors would show reduced size and altered morphology in the frustule of the pennate diatom *Phaeodactylum tricornutum* (Vartanian *et al.*, 2009). That study suggested further investigations to confirm whether VHA directly contributed to the regulation of pH in the SDV, to study the role of VHA in vesicular trafficking and transport of material to the SDV, and to address a potential role of the vacuole in silica biomineralization. However, a subsequent investigation reported the presence of VHA subunit c in the cytoplasm and endoplasmic reticulum (Bussard & Lopez, 2014) rather than the SDV, confounding the potential role of VHA in silicification and suggesting that frustule alteration by VHA inhibitors was an indirect effect. Alternatively, VHA could be present in the silicalemma specifically during frustule formation. Indeed, a change in VHA subcellular localization is a common regulatory mechanism in other organisms; for example, acid/base stress, hormones and neurotransmitters may induce the VHA translocation from the cytoplasm to the cell plasma membrane in kidney (Pastor-Soler *et al.*, 2003), epididymis (Roy *et al.*, 2013), fish gill (Tresguerres *et al.*, 2010; Roa & Tresguerres, 2016), and insect salivary glands (Dames *et al.*, 2006).

To investigate the potential transient location of VHA in the diatom SDV and its role in biomineralization, we generated a transgenic *Thalasiossira pseudonana* cell line expressing VHA subunit B fused to enhanced green fluorescent protein (VHA_B-eGFP). We then took advantage of a synchronization method (Hildebrand *et al.*, 2007) to determine dynamic changes in VHA subcellular location throughout the cell cycle. In the absence of silicon, *T. pseudonana* cannot make new frustules for the daughter cells and the majority of cells arrests in the Gap 1 (G1) stage of interphase. At 4 h after silicon replenishment, *c.* 50% of the cells are in the Gap 2 or mitosis (G2 + M) stages, when cells proceed to perform mitosis, build new valves, and divide (Hildebrand *et al.*, 2007). At 5–8 h after silicon replenishment, the majority of cells in the culture has divided and are in G1 of the next cell division cycle. Frustule biosynthesis was visualized by staining with 2-(4-pyridyl)-5-((4-(2-dimethylaminoethylaminocarbamoyl) methoxy)phenyl)oxazole (PDMPO), an acidotropic dye that selectively incorporates into newly biomineralized silica (Shimizu *et al.*, 2001). VHA activity was downregulated by incubating cell cultures with the highly specific pharmacological inhibitor, concanamycin A (Dröse & Altendorf, 1997; Huss *et al.*, 2002). Higher temporal resolution of VHA_B-eGFP translocation to SDVs was visualized by time-lapse super-resolution confocal microscopy. Additionally, we used *T. pseudonana* expressing SAP1-eGFP fusion proteins to interrogate a putative role of VHA activity on the delivery of silicon-polymerizing proteins to the SDV. Lastly, wild-type *T. pseudonana* cultures were incubated with partial-inhibiting concentrations of concanamycin A and their frustules were imaged using scanning electron microscopy (SEM) to observe effects of VHA activity downregulation on silica biomineralization.

Materials and Methods

Culture conditions

Thalasiossira pseudonana (CCMP1335) cultures were grown axenically in artificial seawater (ASW) medium (Darley &

© 2019 The Authors
New Phytologist © 2019 New Phytologist Trust

Volcani, 1969) supplemented with 1 mM Na_2SiO_3. Wild-type and VHA_B-eGFP expressing cultures were grown on an orbital shaker under continuous illumination by cool-white fluorescent lamps at 70 µmol photons m^{-2} s^{-1} at 18°C. Cell lines expressing SAP1-eGFP were grown under 16 h : 8 h, light : dark conditions to overcome a negative growth phenotype resulting from light-induced overexpression of the SAP1 under control of the fcp-promoter.

Transgenic diatoms expressing fluorescently labeled VHA_B and SAP1

Proteins labeled with eGFP were expressed under the control of the native or fcp promoters. For native expression of Thaps3_40522 (VHA_B), DNA fragments including the full-length coding sequence of the gene, 500 bp upstream of the first methionine, and 500 bp downstream of the stop codon were amplified from *T. pseudonana* genomic DNA, and cloned into the Gateway destination vector pMHL_71 with eGFP at the end of the coding sequence. For fcp expression of Thaps3_40522 (VHA_B) and Thaps3_25736 (SAP1), the full-length coding sequence of the gene was amplified from *T. pseudonana* genomic DNA, and cloned into Gateway destination vector pMHL_79 with eGFP at the end of the coding sequence. All transformation vectors were cotransformed with a pMHL_09 expressing the *nat1* gene which confers nourseothriscin resistance by biolistic gene gun method (Poulsen *et al.*, 2006). Liquid cultures grown in ASW media containing 100 µg ml^{-1} nourseothriscin were enriched for cells expressing eGFP using several rounds of fluorescence-activated cell sorting on a BD Influx Cell Sorter (BD Biosciences, San Jose, CA, USA), from which single colonies expressing eGFP were selected for on ASW agar plates containing nourseothriscin.

Similar localizations were observed in *T. pseudonana* expressing VHA_B-eGFP under control of the native (Supporting Information Fig. S1) and fcp promoters (Fig. 2), indicating that choice of promoter did not influence localization of the fusion protein. However, cells expressing fcp-VHA_B-eGFP were able to be imaged longer by fluorescence microscopy and were used for all experiments involving the VHA_B-eGFP fusion protein.

Synchronized cell cycle localization of VHA_B-eGFP and PDMPO

For synchronization of the cell cycle, starter cultures of *T. pseudonana* expressing fcp-VHA_B-eGFP grown to 2×10^6 cells ml^{-1} were centrifuged at 4000 ***g*** for 10 min and washed twice with silicon-free (Si–) ASW before being resuspended at 1.0×10^6 cells ml^{-1} in 500 ml of Si– ASW. Following 24 h of silicon starvation, sodium silicate was added at 200 µM final concentration to initiate cell-cycle progression, and PDMPO; LysoSensor YellowBlue DND-160 (Life Technologies, Carlsbad, CA, USA), an acidotropic silica biomineralization marker, was added at 0.125 µM final concentration to visualize low-pH compartments and newly synthesized biosilica. VHA_B-eGFP and PDMPO localization were tracked in cells sampled from $t = 0$ to $t = 8$ h at the start of each hour by fluorescence microscopy on a Zeiss Axio Observer.Z1 inverted microscope. Visual analysis and calculations of VHA and PDMPO localization were carried out by recording cells with eGFP signal and/or PDMPO signal in the valve SDV out of the total cell population using the CELL COUNTS plugin in FIJI (Schindelin *et al.*, 2019). In parallel experiments, 2.5 µl of a 1 mM concanamycin A (AdipoGen BVT-0237; ≥ 98% purity) stock solution prepared in dimethyl sulfoxide (DMSO) was added at 5 nM to 500 ml cell cultures to inhibit VHA activity (Dröse & Altendorf, 1997; Bowman & Bowman, 2002; Huss *et al.*, 2002); equal volumes of DMSO were added in control experiments to account for potential side-effects of DMSO on diatom cells. The filter sets used for GFP was Zeiss #38HE (Ex 470/40 nm, FT 495 nm, Em 525/50 nm), for PDMPO was Zeiss #21HE (Ex 387/15 nm, FT 409 nm, Em 510/90 nm), and for Chl autofluorescence was Zeiss #05 (Ex 395-440 nm, FT 460 nm, Em 470 nm).

Super-resolution confocal microscopy

For single-cell time-lapse imaging, 2 ml of exponentially growing *T. pseudonana* cell culture expressing VHA_B-eGFP was transferred to a 35 mm poly-d-lysine-coated glass-bottom Petri dish. Cells were allowed to adhere to the Petri dish bottom for 15 min followed by the addition of 2 ml of ASW medium and PDMPO was added for a final concentration of 0.125 µM. Dishes were mounted on a Warner Instruments (Camden, CT, USA) QE-1HC Quick Exchange Heated/Cooled stage chamber controlled by CL-200 Dual Channel Temperature Controller maintained at 18°C. Cells were imaged with a Zeiss LSM800 inverted confocal microscope equipped with a Zeiss Plan-Apochromat ×63 (1.4) Oil DIC M27 objective, and Zeiss Airyscan super-resolution detector. Two channels were acquired to monitor eGFP (Ex 488 nm with 0.5% laser power, Em 509 nm, detection 490–535 nm) and PDMPO (Ex 335 nm at 0.6% laser power, Em 530 nm, detection 490–575 nm) fluorescence. Images were collected at 3 min intervals for 4 h with Zeiss Definite Focus stabilization enabled.

VHA_B mRNA expression

Thaps3_40522 (VHA_B) mRNA expression level fragments per kilobase per million reads mapped (FPKM) was acquired from transcriptomics analysis of RNAseq data collected from time-course experiments following silicon replenishment from biological duplicates of synchronized *T. pseudonana* cultures (Abbriano Burke, 2017). Raw reads from individual samples were demultiplexed based on a perfect barcode match, and TOPHAT (v.2.0.6) running BOWTIE 2 (v.2.0.2) was used for strand-specific mapping of RNAseq reads to the *T. pseudonana* reference genome assembly (Thaps3) obtained from the Joint Genome Institute (JGI): (http://genome.jgi.doe.gov/Thaps3/Thaps3.download.ftp.html). CUFFLINKS (v.2.2.1) was used to assemble transcripts, and the assembly was used for AUGUSTUS gene model prediction. Raw counts to AUGUSTUS-generated gene models were generated using HTSEQ-COUNT (HTSEQ 0.6.1p1). Normalized counted and

© 2019 The Authors
New Phytologist © 2019 New Phytologist Trust

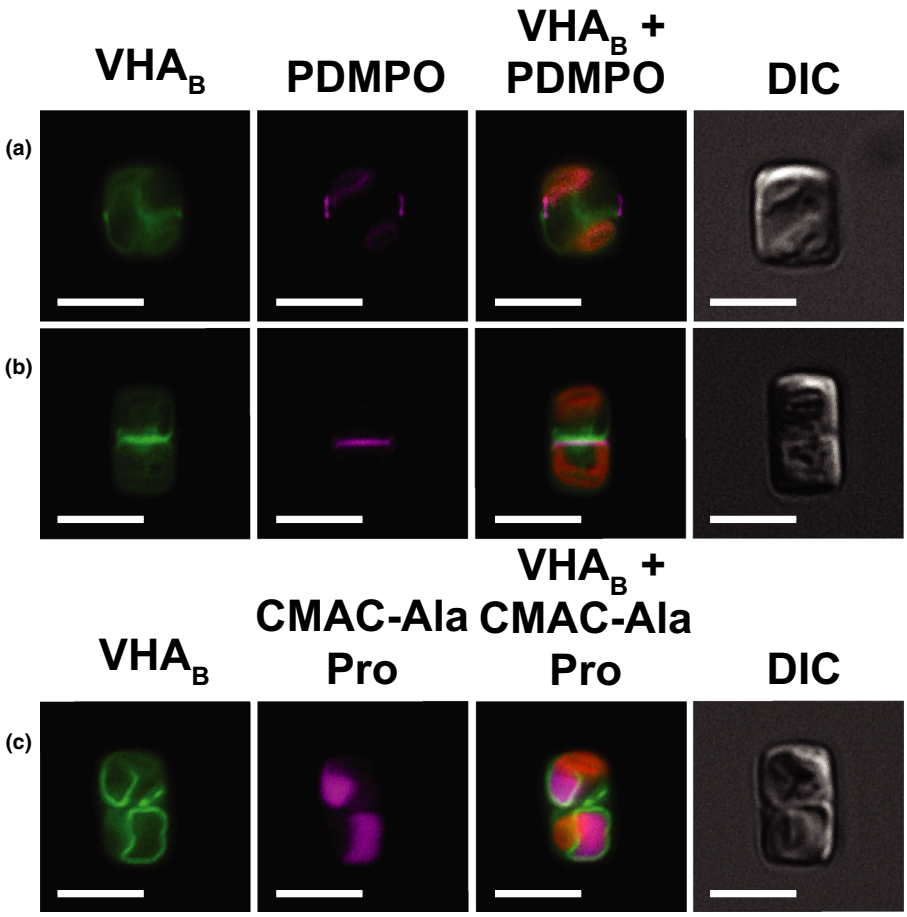


Fig. 2 V-type H^+-ATPase (VHA) localization in multiple subcellular compartments. Representative images of exponentially growing *Thalassiosira pseudonana* expressing fcp-VHA B subunit tagged with enhanced green fluorescent protein (fcp-VHA_B-eGFP) in: (a) a girdle band silica deposition vesicle (SDV); (b) valve SDVs; and (c) vacuole tonoplast. Green, VHA_B-eGFP; red, Chl; magenta, 2-(4-pyridyl)-5-((4-(2-dimethylaminoethyl-aminocarbamoyl) methoxy)phenyl)oxazole (PDMPO) (a, b), CMAC-Ala-Pro (c); white, colocalization of VHA_B-eGFP and PDMPO (a, b). Bars, 5 μm.

differential expression analysis was done using the DESeq2_1.6.3 package.

VHA_B protein abundance

Subsamples of synchronized wild-type *T. pseudonana* expressing VHA_B-eGFP were harvested at $t = 0$ before silicon replenishment, and every hour thereafter ($t = 1$–8 h), by centrifugation at maximum speed at 4°C for 5 min followed by freezing of the pellet on dry ice. Protein was extracted in a 2× Extraction Buffer (125 mM Tris, pH 6.8, and 138 mM sodium dodecyl sulfate) by boiling at 95°C for 5 min, pelleting at maximum, speed, and recovering the supernatant for Western blot analysis. Protein concentration was determined with the Bio-Rad D/C Protein Assay Kit and BSA protein standard. Western blots were performed by separating 23 μg of total protein in a 10% polyacrylamide mini gel (60 V, 20 min; 120 V, 90 min) and transferring to a polyvinylidene difluoride (PVDF) membrane. Equivalent protein loading was confirmed by Ponceau staining of total protein on the PVDF membranes (Romero-Calvo *et al.*, 2010). Membranes were blocked in 3% milk-blocking buffer and incubated with custom monoclonal VHA_B primary antibody (1 : 100) at 4°C overnight. Membranes were washed three times with Tris-buffered saline + 0.1% TWEEN 20 (T-BST) and incubated with goat-anti-mouse horseradish peroxidase antibody (1 : 10 000) at room temperature for 1 h. Membranes were developed with Bio-Rad Western Clarity ECL and analyzed in a Bio-Rad Universal III Hood using ImageQuant software (Bio-Rad, Hercules, CA, USA).

SEM imaging of frustules

Wild-type *T. pseudonana* synchronized by silicon starvation was incubated with 200 μM Na_2SiO_3 for 2 h, then exposed to 0 (control), 0.4, 1.0, and 2.0 nM concanamycin A for 22 h. At $t = 24$ h, 20 ml of each cell culture was pelleted and frozen on dry ice. Frustules were acid-washed by resuspending pellets in 50 μl of milli-Q H_2O (resistivity of 18.2 MΩ cm at 25°C) and vortexing with 200 μl 100% H_2SO_4. Samples were then boiled for 10 min, cooled on ice before adding a small amount of KNO_3, and boiled again for 10 min. Next, 800 μl of H_2O was added to samples before centrifuging at 1500 ***g*** for 10 min; the supernatant was discarded. These steps were repeated, without vortexing, to remove all intracellular contents. After washing with H_2O three times, frustules were resuspended in 200 ml of 100% ethanol for storage and air-dried onto stubs at ambient conditions for SEM imaging. Acid-cleaned frustules were imaged on Zeiss Sigma 500 SEM at the California Institute for Telecommunications and Information Technology Nano3 facility at UCSD. Quantification of normal and altered valves was completed using the CELL COUNTS plugin in Fiji (Schindelin *et al.*, 2019).

© 2019 The Authors
New Phytologist © 2019 New Phytologist Trust

Results

Subcellular localization of VHA_B-eGFP in *T. pseudonana*

Diatoms expressing VHA_B-eGFP under control of the fcp promoter from exponentially growing (i.e. not synchronized) cultures displayed heterogeneous VHA_B-eGFP subcellular localization. VHA_B-eGFP was generally found faintly throughout the cytoplasm in all cells. In addition, more concentrated VHA_B-eGFP signal was present in the silicalemma of girdle band SDVs (Fig. 2a) and valve SDVs of dividing cells (based on colocalization with PDMPO; Fig. 2b) or in vacuole tonoplasts (based on colocalization with the vacuolar marker CMAC Ala-Pro; Fig. 2c).

VHA_B mRNA and protein expression in synchronized cell cultures

Next, we quantified VHA_B mRNA and protein abundance along the cell cycle of *T. pseudonana* cultures synchronized by silicon starvation and replenishment (Fig. 3). Expression of mRNA was measured using an Illumina (La Jolla, CA, USA) HiSeq 2000 sequencer. VHA_B mRNA had a peak at $t = 4$ h that was *c.* 3.2-fold higher compared with $t = 0$ h (4501 vs 1391 FPMKs). VHA_B mRNA abundance then decreased to basal values (*c.* 1116 FPKMs) by $t = 8$ h. Expression of VHA_B protein was quantified by Western blotting and revealed two bands, one at *c.* 55 kDa (corresponding to native VHA_B) and another at *c.* 88 kDa (corresponding to transgenic VHA_B plus the 33 kDa eGFP tag) (Fig. S2). Native VHA_B protein abundance had a *c.* 3.2-fold peak between $t = 3$ h and $t = 5$ h (Fig. 3). The Western blots also showed that the level of VHA_B-eGFP protein overexpression over native VHA_B was moderate, with a maximum of *c.* 2.4-fold at $t = 1$ h and nearly equal levels from $t = 4$ h and onwards.

These mRNA and protein abundance peaks occurred between $t = 4$ h and $t = 5$ h, which coincided with initiation of valve formation and maximum cell length during the G2 + M phase of the cell cycle observed in previous synchrony experiments conducted with *T. pseudonana* (Hildebrand *et al.*, 2007). While this pattern of VHA_B expression is consistent with synthesis of new VHA_B protein for valve SDVs, the presence of VHA_B in multiple subcellular localization shown in Fig. 2 prevents assessment of its significance to cell physiology.

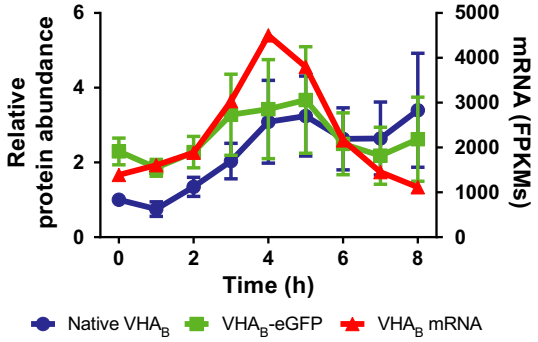


Fig. 3 Relative VHA B subunit (VHA_B) protein abundance ($n = 5$, error bars = ± SE) and mRNA expression (FPKM) from synchronized *Thalassiosira pseudonana* cultures following silicon replenishment. FPKM, fragments per kilobase per million reads mapped.

VHA_B-eGFP and PDMPO localization in SDVs of synchronized cells

To investigate the physiological role of VHA throughout the cell cycle of *T. pseudonana*, VHA_B-eGFP subcellular localization was tracked alongside frustule morphogenesis using the acidotropic silica biomineralization marker PDMPO using fluorescence microscopy. In synchronized cultures, analysis of PDMPO accumulation in the valve SDV in control and concanamyin A-treated cells (Fig. 4a) revealed a strong relationship between VHA_B-eGFP translocation to the valve SDV, valve formation, and progression of the cell cycle. In the period $t = 0$–3 h after silicon replenishment, VHA_B-eGFP and PDMPO signals in the valve SDV were minimal, with both occurring in *c.* 5% of the population. The observed peak of roughly one-third of the cell population exhibiting both VHA_B-eGFP and PDMPO in the valve SDV at $t = 4$ h matches previous reports that the majority of synchronized *T. pseudonana* begin synthesizing the valves at 3.5 h after silicon replenishment (Hildebrand *et al.*, 2007). At $t = 5$ h, PDMPO signal in newly synthesized valves increased to *c.* 67% and reached a maximum of *c.* 88% after $t = 7$ h. However, VHA_B-eGFP signal in the valve SDV decreased to *c.* 14% of the cells at $t = 5$ h, and then to a minimum of *c.* 2% by $t = 8$ h. This is consistent with VHA leaving the silicalemma after the completion of valve synthesis.

Dynamics of VHA_B-eGFP localization and silica biomineralization in SDVs of synchronized cells

Fig. 4(b) shows representative VHA_B-eGFP expressing cells corresponding to the hours following silicon replenishment and phases of the cell cycle. In the G1 phase ($t = 0$–2 h) following silicon replenishment, VHA_B-eGFP was present throughout the cytoplasm and more prominently in vacuole tonoplasts (Fig. 4bi). Further along in the G1 phase, VHA_B-eGFP was present in a single girdle band SDV which colocalized with PDMPO, marking newly synthesized girdle bands (Fig. 4bii). At the beginning of the G2 + M phase ($t = 3$–6 h), VHA_B-eGFP accumulated along with a diffuse signal from PDMPO in the middle of the cell where valve synthesis occurs (Fig. 4biii). Further into the G2 + M phase, VHA_B-eGFP was present in the valve SDVs while PDMPO signal became concentrated and bound within the newly synthesized valves (Fig. 4biv). VHA_B-eGFP was maintained in valve SDVs as valve synthesis neared completion (Fig. 4bv). By the end the G2 + M phase, the new PDMPO-labeled valves were exocytosed and the two cells divided. As the daughter cells transitioned to the next G1 phase ($t = 6$–8 h), VHA_B-eGFP was again present in girdle band SDVs while a majority of VHA_B-eGFP was present in tonoplasts, presumably to serve in physiological functions carried out by vacuoles (Fig. 4bvi).

Having established a clear relationship between VHA and SDVs, the functional effect of abolishing VHA activity using the

© 2019 The Authors
New Phytologist © 2019 New Phytologist Trust

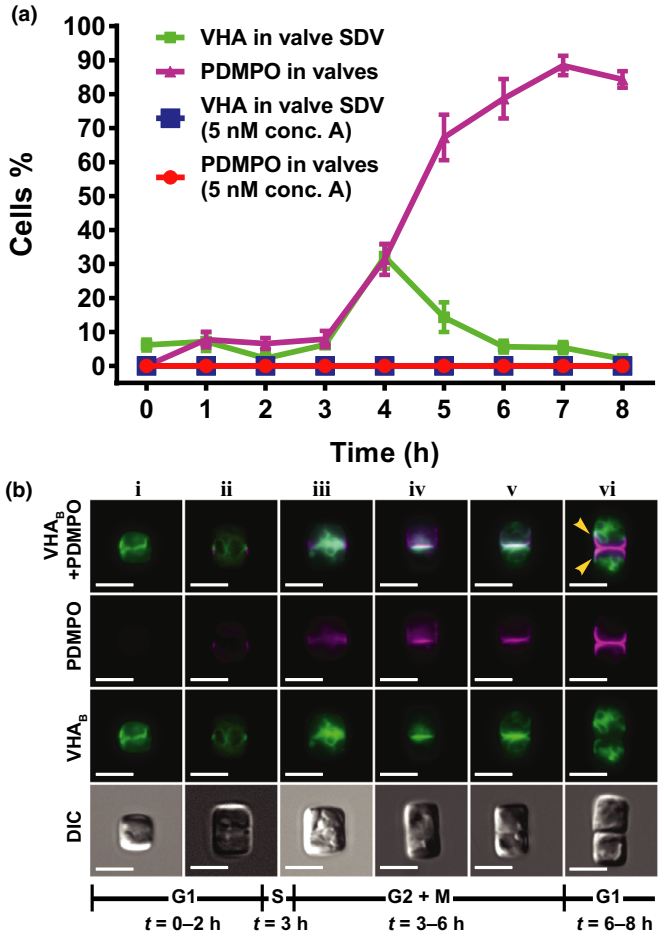


Fig. 4 (a) V-type H^+-ATPase (VHA) dynamics in the valve-specific silica deposition vesicles (SDVs) throughout the cell cycle. Percentage of cells with VHA B subunit tagged with enhanced green fluorescent protein (VHA_B-eGFP) in the valve-specific SDVs, and 2-(4-pyridyl)-5-((4-(2-dimethylaminoethyl-aminocarbamoyl) methoxy)phenyl)oxazole (PDMPO) signal in valves in control and concanamycin A (conc. A)-treated cultures. VHA and PDMPO localization were analyzed using the CELL COUNTER tool in IMAGEJ on *c.* 280 cells per time point (*c.* 2500 cells total; $n = 3$; error bars are ± SE). (b) Representative cell images of VHA_B subcellular localization throughout the cell cycle in *Thalassiosira pseudonana* expressing fcp-VHA_B-eGFP: (i) cytoplasmic and tonoplast localization; (ii) tonoplast and girdle band SDV localization during G1 phase; (iii) accumulation at the site of valve biosynthesis; (iv, v) initial (iv) and later stage (v) concentration in the valve SDVs during the G2 + M phase; (vi) cytoplasmic, girdle band SDV, and tonoplast localization in the G1 phase of two daughter cells. Green, VHA_B-eGFP; magenta, PDMPO; white, colocalization of VHA_B-eGFP and PDMPO; red, Chl; DIC, differential interference contrast. Yellow arrows in (vi) indicate girdle bands. Bars, 5 μm.

highly specific inhibitor concanamycin A (5 nM) was investigated. Cell cultures treated with concanamycin A displayed no VHA_B-eGFP signal in SDVs throughout the synchronized time-course (Fig. 4a). Concanamycin A also prevented the accumulation of PDMPO in valves throughout the time-course (Fig. 4a), which indicated that frustule biosynthesis was inhibited and was consistent with the lack of cell division even after 24 h of exposure to the drug. Cells exposed to concanamycin A showed VHA_B-eGFP distributed as a diffuse signal throughout the cytoplasm with a slightly denser signal in the middle of the cell, but lacking the concentrated signal typical of intracellular membrane labeling (Fig. 5a–c). Additional images of concanamycin A-treated cells are shown in Fig. S3.

Live cell time-lapse imaging of VHA_B-eGFP dynamics

The dynamics of VHA_B-eGFP translocation in SDVs was investigated using time-lapse super-resolution confocal fluorescence microcopy analysis of single *T. pseudonana* cells expressing fcp-VHA_B-eGFP incubated with PDMPO during the G2 + M phase (corresponding to $t = 4$ h of the synchrony, and defined here as $t = 0$ min) (Fig. 6). At $t = 0$ min, VHA_B-eGFP was predominantly in the tonoplasts of two adjacent vacuoles. At $t = 6$ min, a distinct VHA_B-eGFP signal began to accumulate at the center of the cell marking the membranes of two adjacent valve SDVs. Three minutes later, at $t = 9$ min, PDMPO began to mark new valves and VHA_B-eGFP signal expanded further along the middle region of the cell. By $t = 27$ min, VHA_B-eGFP had made its way across the entire middle plane and a strong colocalization with PDMPO became visible. By $t = 66$ min the VHA signal in the SDVs began to decrease while PDMPO remained trapped within mature valve biosilica. At $t = 93$ min, VHA_B-eGFP signal in the SDV was nearly absent, and by $t = 111$ min, VHA_B-eGFP was only faintly visible in the plasma membrane of each daughter cell. VHA_B-eGFP signal was always present in vacuole tonoplasts which appeared to be associated with the valve SDVs up until $t = 93$ min. A movie of this time-lapse can be found in Video S1.

The VHA_B-eGFP dynamics in girdle band SDVs was captured in two attached daughter cells in the G1 phase (Fig. 7). This approach was adopted to consistently identify cells in the G1 phase following valve biosynthesis in the G2 + M phase for high-magnification focusing for super-resolution imaging. At $t = 0$ min, each cell already had newly synthesized girdle bands which extend from the valves and are labeled with PDMPO. In the top cell, VHA_B-eGFP was concentrated in the vacuole tonoplasts which could be seen in close association with a new girdle band SDV (similar to the association with the valve SDVs show in Fig. 6). In the period $t = 24$–57 min, VHA_B-eGFP colocalized with PDMPO in girdle band SDVs. By $t = 60$ min, VHA_B-eGFP had left the girdle band SDV while PDMPO remained in the newly synthesized girdle band. Similar observations were made in the lower cell, but it was delayed by *c.* 10 min relative to the top cell. A movie of this time-lapse showing the completion of both upper and lower girdle bands can be found in Video S2.

Effects of VHA inhibition on SAP1 incorporation into the SDV

Next, we examined whether VHA activity is required for the incorporation of the structural protein SAP1 into SDVs in cultures of *T. pseudonana* expressing fcp-SAP1-eGFP. First, we confirmed the previously described localization of SAP1 (Tesson *et al.*, 2017) in the silicalemmas of SDVs of both girdle bands (Fig. 8a) and valves (Fig. 8b). In dividing cells, SAP1 appeared to be trafficked through the cytoplasm in a single

© 2019 The Authors
New Phytologist © 2019 New Phytologist Trust

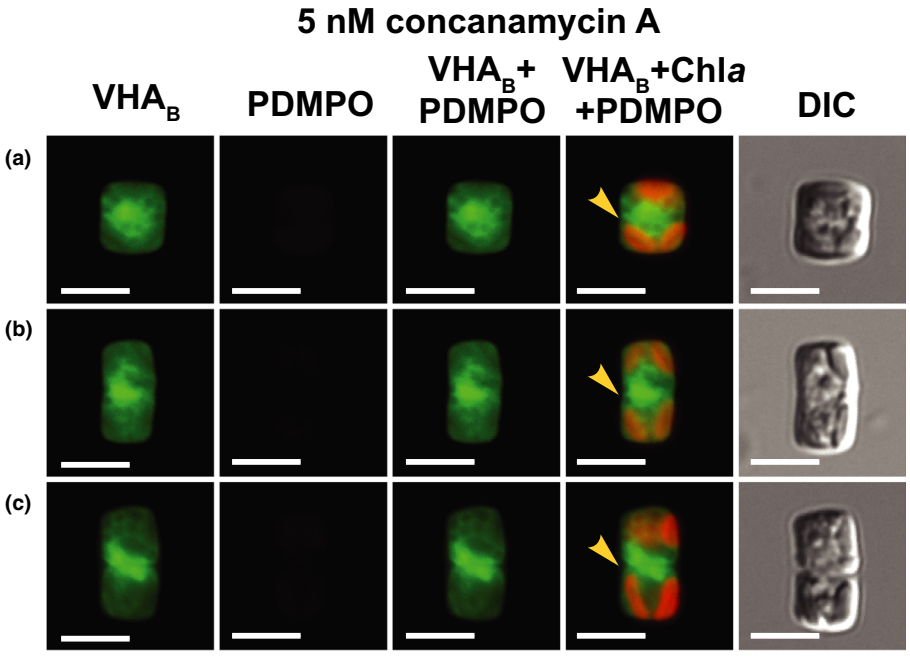


Fig. 5 Inhibition of V-type H^+-ATPase (VHA) activity prevents frustule biosynthesis. (a–c) Representative images of synchronized *Thalassiosira pseudonana* expressing fcp-VHA B subunit tagged with enhanced green fluorescent protein (fcp-VHA$_B$-eGFP) treated with 5 nM concanamycin A. Green, VHA$_B$-eGFP; magenta, 2-(4-pyridyl)-5-((4-(2-dimethylaminoethyl-aminocarbamoyl) methoxy)phenyl)oxazole (PDMPO); white, colocalization of VHA$_B$-eGFP and PDMPO; red, Chl; DIC, differential interference contrast. Yellow arrowheads highlight VHA accumulation near the location where the valve biosynthesis normally occurs. Bars, 5 μm.

vesicle that attached to valve SDVs and fused into the silicalemma (Fig. S4a–f). Following cytokinesis, SAP1 was again found within a single vesicle adjacent to newly formed valves in each daughter cell (Fig. 8c). However, in cells exposed to 5 nM concanamycin A, SAP1 accumulated in the middle of the cell, in multiple vesicles that varied in size (Figs 8d–f, S4g–l). Similar to the VHA inhibition experiments captured in Figs 4(a) and 5, 5 nM concanamycin A prevented PDMPO accumulation in SDVs, indicating inhibition of frustule biosynthesis. However, intense PDMPO signal was observed in a few SAP1-containing vesicles (Fig. 8f), suggesting they were acidic and that silica may have biomineralized in those compartments despite VHA inhibition. We tentatively suggest this is related to SAP1 overexpression.

Effects of VHA inhibition on valve nanostructure

Finally, we exposed *T. pseudonana* cultures to submaximal concanamycin A concentrations (0–2 nM) to examine the effects of reduced VHA activity on growth and valve ultrastructure. A dose–response growth curve revealed that cultures exposed to 0.4 nM concanamycin A resulted in a *c.* 25% decrease in growth rate and *c.* 36% decrease in final cell density compared with the control treatment (Fig. 9a). About one-quarter of the valves from diatoms exposed to 0.4 nM concanamycin displayed altered morphology, while the remaining valves were probably synthesized before exposure to concanamycin A and therefore looked normal. Compared with valves from control diatoms (Fig. 9b), altered valves exhibited decreased deposition of silica, and lacked features

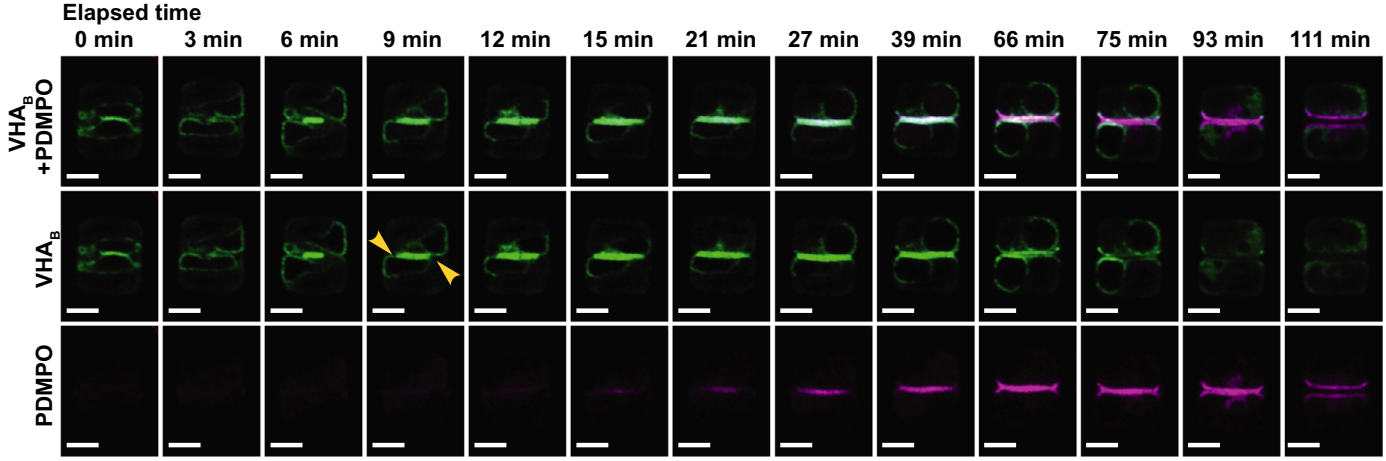


Fig. 6 Time-lapse during valve biosynthesis. Selected images from time-lapse super-resolution confocal fluorescence microscopy of *Thalassiosira pseudonana* expressing fcp-VHA B subunit tagged with enhanced green fluorescent protein (fcp-VHA$_B$-eGFP) incubated with 2-(4-pyridyl)-5-((4-(2-dimethylaminoethyl-aminocarbamoyl) methoxy)phenyl)oxazole (PDMPO) are shown during valve biosynthesis (Supporting Information Video S1). Green, VHA$_B$-eGFP; magenta, PDMPO; white, colocalization of VHA$_B$-eGFP and PDMPO. Yellow arrowheads highlight association of vacuoles with silica deposition vesicles (SDVs). Bars, 2.5 μm.

© 2019 The Authors
New Phytologist © 2019 New Phytologist Trust

characteristic of the distal surface of valves (Fig. 9c–e). While ribs were present in the altered valves, they lacked defined ridges and were composed of more granular silica nanoparticles. As a result of reduced silica deposition, some of the valves were bent at the edges making them less round (Fig. 9c), suggesting a decrease in rigidity. The portula was also deformed and the fultoportulae were mislocated away from the outer edges, and found closer to the center of the valve (Fig. 9c). Suboptimal VHA activity additionally affected the nanopore-containing space in between ribs (Fig. 9e): in some frustules it was only partially filled, and in the most extreme cases it was entirely absent. Additional images of altered valves are shown in Fig. S5.

Discussion

Our results demonstrate that VHA is responsible for the acidification of *T. pseudonana* SDVs which is essential for silica biomineralization *in vivo*, and identify the dynamic translocation of VHA to SDVs as a novel mechanism for frustule biosynthesis. Combining transgenic diatoms expressing VHA_B-eGFP and synchronization of the cell cycle by silicon depletion and replenishment allowed us to study the order of events that led to SDV acidification, silicon biomineralization and cell division. Under our experimental conditions, the average duration of the cell cycle is *c.* 8 h. During G1 (t = 0–2 h after silicon replenishment), VHA_B-eGFP is found in the cytoplasm and concentrated in vacuole tonoplasts and then to girdle band SDVs for the synthesis of girdle bands which expand the cell. At the onset of G2 and during mitosis (t = 3–6 h), VHA_B-eGFP translocates from vacuoles to valve SDVs of each daughter cell to produce the two new valves required for the cells to separate. Time-lapse imaging using super-resolution confocal microscopy showed that VHA_B-eGFP presence in the SDV precedes accumulation of the acidotrophic dye PDMPO, which in turn is completely abolished by the highly specific VHA inhibitor concanamycin A. Altogether, this indicates that VHA acidifies the SDV and that this acidification is essential for frustule biosynthesis. After the new valves are exocytosed (t = 6–8 h), cells enter G1 of the next cell cycle and VHA_B-eGFP is turned over by translocating to the plasma membrane, leaving behind PDMPO-labeled frustules and confirming the dynamic nature of VHA. These results support the previous suggestion that the SDV integrate with the plasma membrane after frustule exocytosis (Kotzsch *et al.*, 2017).

The essential role of VHA activity on diatom frustule formation is a result of at least two potential processes. First, VHA probably provides the acidic pH that has long been predicted inside the SDV which may aide in shaping and arranging silica nanospheres, and enabling the proper function of silica-forming proteins (Iler, 1979; Kröger *et al.*, 1999, 2000, 2002; Sumper & Kröger, 2004; Kotzsch *et al.*, 2017). Although P-type H^+-ATPases have been identified in diatoms (Bussard & Lopez, 2014), they are not inhibited at the nanomolar concentrations of concanamycin A used in our study (Dröse & Altendorf, 1997). Given the specificity of concanamycin A for VHA, and its suppressive effect on frustule synthesis as well as cell division in cultures, our results suggest that VHA is the only proton pump involved in SDV acidification. Second, VHA inhibition blocked the delivery of SAP1-containing vesicles to SDVs, pointing out a potential role of VHA in regulating vesicle fusion to the silicalemma. This function may depend on SDV acidification itself

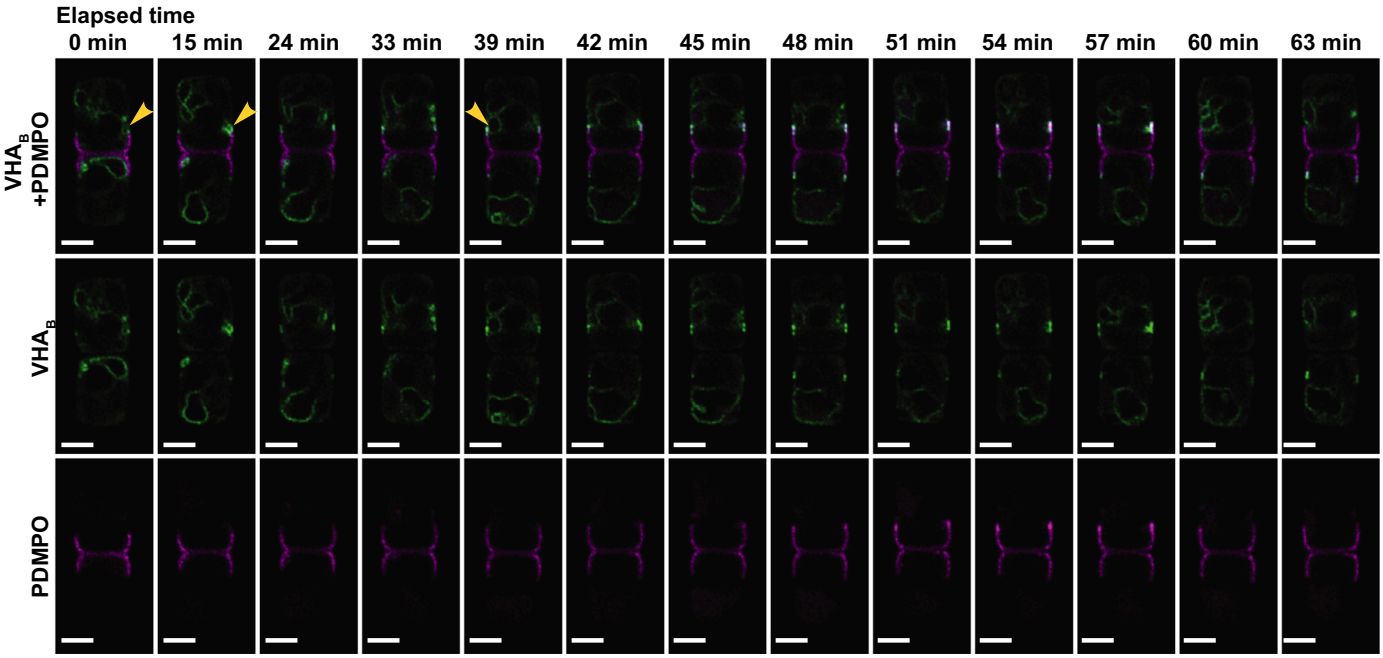


Fig. 7 Time-lapse during girdle band biosynthesis. Selected images from time-lapse super-resolution confocal fluorescence microscopy of two attached *Thalassiosira pseudonana* cells expressing fcp-VHA B subunit tagged with enhanced green fluorescent protein (fcp-VHA_B-eGFP) incubated with 2-(4-pyridyl)-5-((4-(2-dimethylaminoethyl-aminocarbamoyl) methoxy)phenyl)oxazole (PDMPO) are shown during girdle band biosynthesis (Supporting information Video S2). Green, VHA_B-eGFP; magenta, PDMPO; white, colocalization of VHA_B-eGFP and PDMPO. Yellow arrowheads highlight association of vacuoles with SDVs. Bars, 2.5 μm.

© 2019 The Authors
New Phytologist © 2019 New Phytologist Trust

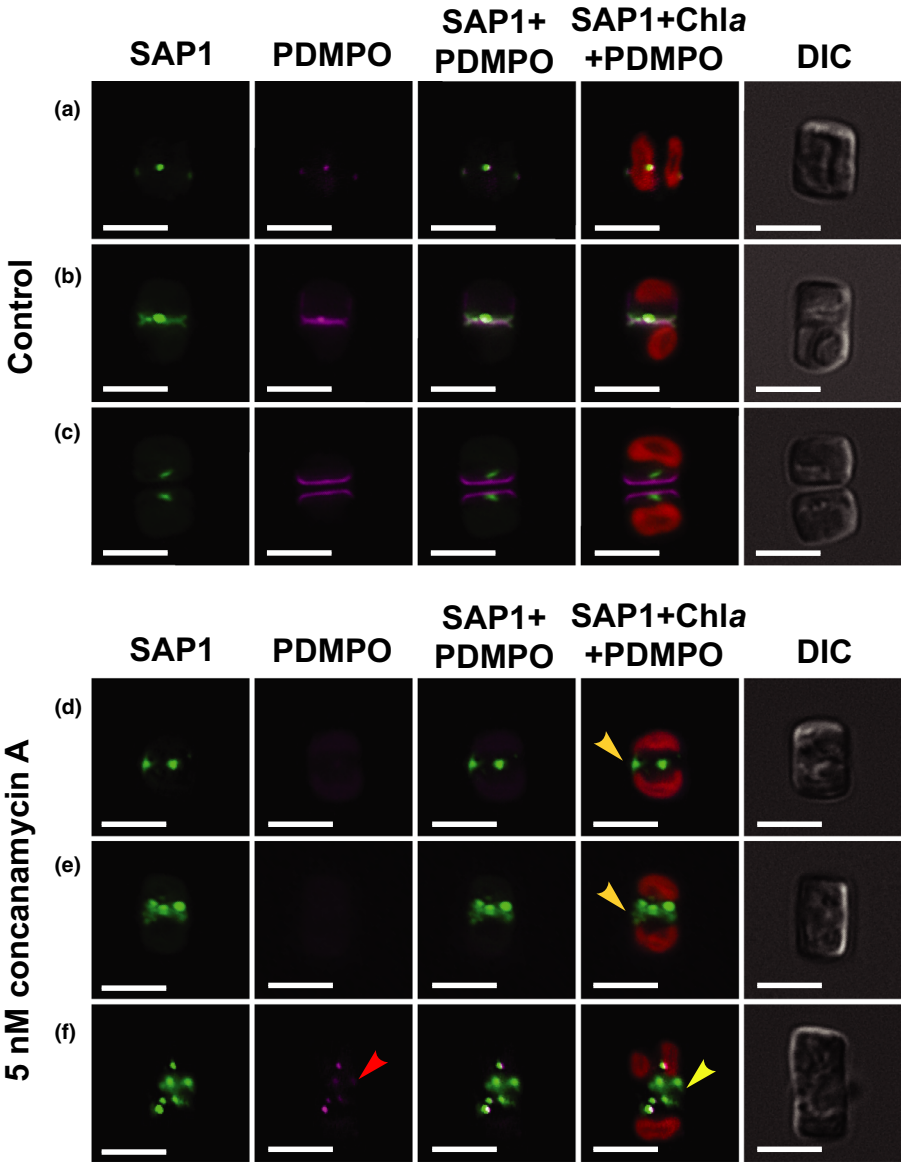


Fig. 8 Inhibition of V-type H^+-ATPase (VHA) activity prevents insertion of SAP1 into the silica deposition vesicle (SDV). Representative images of cell cycle-synchronized *Thalassiosira pseudonana* expressing fcp-SAP1-eGFP. (a–c) Control cells; (d–f) cells incubated with 5 nM concanamycin A. Green, SAP1-eGFP; magenta, 2-(4-pyridyl)-5-((4-(2-dimethylaminoethyl-aminocarbamoyl) methoxy)phenyl)oxazole (PDMPO); white, colocalization of SAP1-eGFP and PDMPO; red, Chl; DIC, differential interference contrast. Yellow arrowheads highlight SAP1 near the location where the valve biosynthesis normally occurs; the red arrow highlights the concentration of PDMPO in SAP1 vesicles. Bars, 5 μm.

or on the recruitment of the vesicle fusion machinery by VHA as reported in other cells (Maxson & Grinstein, 2014). If this is true, another outstanding question is whether VHA activity is required for the fusion of vesicles trafficking other components to the SDV of newly forming frustules, including other structural proteins found in SDV membranes and substrates of the insoluble organic matrices known to comprise frustules (Tesson & Hildebrand, 2013; Kotzsch *et al.*, 2016). Alternatively, inhibition of VHA by concanamycin A may prevent SDV formation, leaving SDV-associated proteins without a final location to target to.

In addition to the SDV, we found that VHA_B-eGFP is present in the vacuole tonoplast in cells in various cell stages (Figs 2c, 4b, 6, 7), which opens new questions about the regulatory mechanisms behind differential VHA subcellular localization and coordination of vacuolar function and cell division. Interestingly, the tonoplast appeared to maintain an association with the SDV, and may act as a reservoir for newly synthesized VHA. The proximity of vacuoles near locations of valve and girdle band synthesis suggests the transfer of VHA-containing tonoplast to the silicalemma during valve biogenesis, providing insights into the potential origin of SDV membrane material such as lipids and other proteins. In cultures treated with a fully inhibiting dose of concanamycin A, cells that were in the process of dividing had increased VHA_B-eGFP in the site where the new valves would form; however, they lacked a defined SDV (Figs 5a–c, S3). In these cells, we hypothesize that VHA_B-eGFP was localized in a nonrigid SDV membrane representative of an early stage in valve formation, which is consistent with previous observations of very early stages of valve formation with deformed but recognizable silica structure (Hildebrand, 2010) and a folded appearance similar to a 'taco' shell (Hildebrand *et al.*, 2007). An interesting concept to consider is whether the normal SDV shape directly depends on VHA activity. To prevent aberrant valve structure, the SDV must become fully expanded before or at least concurrent with completion of the base layer. Thus, SDV expansion would be a property of the organic material comprising the SDV,

© 2019 The Authors
New Phytologist © 2019 New Phytologist Trust

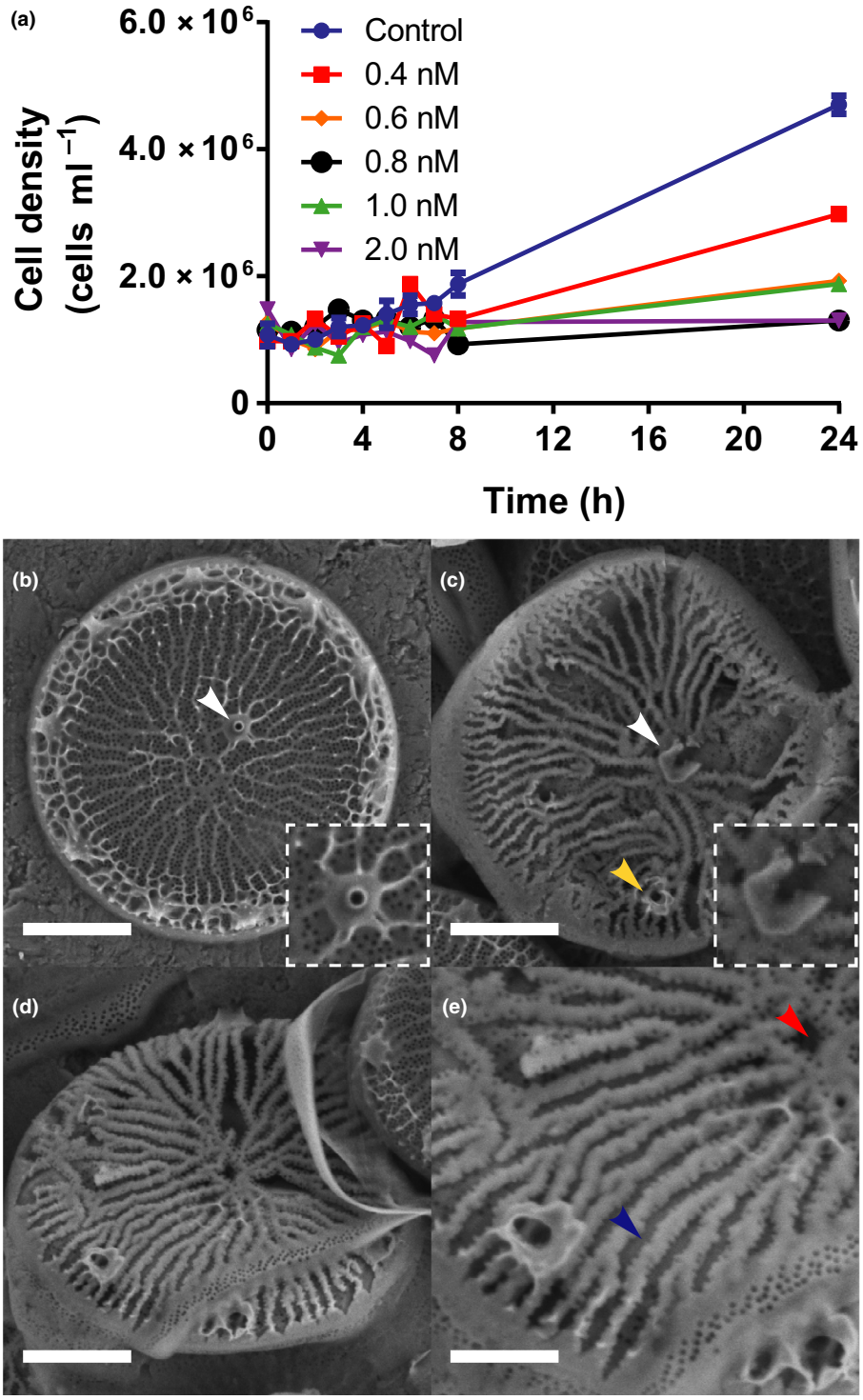


Fig. 9 Suboptimal V-type H^+-ATPase (VHA) activity results in abnormal valve nanostructure. (a) Growth curves of *Thalassiosira pseudonana* cultures under various concanamycin A concentrations ($n = 2$; error bars are ±SE). Valve nanostructure was examined by scanning electron microscopy after 22 h growth in control (b) or 0.4 nM concanamycin A (c–e) conditions. (b, c) Insets shows central portula at ×2 magnification; white arrowheads, central portula; (c) yellow arrowhead, displaced fultoportula; (e) blue arrowhead, ribs lacking ridges; red arrowhead, unfilled nanopore base layer. Bars: 1 μm (b–d); 0.5 μm (e).

and not the silica itself. In addition, several *T. pseudonana* silicification proteins exhibit reversible aggregation as pH is decreased (Kotzsch *et al.*, 2016, 2017), suggesting that VHA-dependent acidification induces protein aggregation and organization inside the SDV, resulting in a subsequent change in SDV topology and expansion.

The halting of cell division by a high concanamycin A dose together with the presence of VHA_B-eGFP in multiple subcellular compartments unfortunately prevented the generation of VHA gene knockouts as a result of lack of growth and potential unspecific effects on other physiological processes, respectively. As an alternative, we examined the effect of VHA pharmacological knockdown on valve morphology by growing synchronized *T. pseudonana* cultures in a partially inhibiting concanamycin A dose. These cells divided at *c.* 75% of the normal rate which yielded a mix of normal valves that were generated before the addition of concanamycin A, and newly formed valves with an abnormal morphology. While the ribs in the silica base layer had

© 2019 The Authors
New Phytologist © 2019 New Phytologist Trust

relatively minor malformations, the nanopore network in the areas between the ribs was partially or entirely missing, and the portula and fultoportulae were deformed and occasionally displaced from their normal locations. These results suggest that a fully acidified SDV is more essential for maturation of the distal surface ridges above the ribs of the valves and porous base layer of nanopores. Interestingly, a SAP1 knockdown (Tesson *et al.*, 2017) and Sin1 knockout (Görlich *et al.*, 2019) also resulted in aberrant patterning deposition of the silica network in the distal valve surface, further supporting the link between VHA function and recruitment of SAP1-containing vesicles to the SDV.

Conclusion

This study confirms the decades-long hypotheses (Gordon & Drum, 1994) that VHA is the enzyme directly responsible for SDV acidification *in vivo*. It also identified that VHA activity regulates the trafficking and fusion of vesicles containing the structural protein SAP1 into the SDV, and revealed that frustule formation is a highly dynamic process that includes intimate interactions between SDVs and vacuoles. In addition to revealing those novel basic mechanistic aspects of diatom frustule biosynthesis, this study has identified interesting areas for future research. Is VHA activity important for the trafficking of other proteins to the SDV or biogenesis of the SDV? What is the function of VHA in the vacuole? What are the regulatory mechanisms behind differential VHA subcellular localization throughout the cell cycle? Can we take advantage of this information to manipulate VHA activity and nanoengineer frustules with specific porosity, silica nanosphere size and ornamentation?

The dominance of diatoms over other phytoplankton groups is presumed to be due, in part, to their ability to use silica as a substrate for growth. Compared with carbon, making cell walls out of silica provides energy savings (Raven, 1983), and silica cell walls have been proposed to act as a pH buffer to provide more CO_2 and promote photosynthesis (Milligan & Morel, 2002). Thus, understanding the mechanisms responsible for diatom silicification carries broader implications for understanding the role of diatoms in the global carbon cycle and primary production in the oceans.

Acknowledgements

The project described was supported by awards from the National Institute of Health Training Grant in Marine Biotechnology (T32GM067550) and the Edna Bailey Sussman Foundation to DPY, and the UCSD Frontiers of Innovation Scholars Program to MT. We would like to thank Dr Roshan Shreshta for providing plasmids and assisting with diatom cloning and transformations, Dr Raffaela Abbriano Burke for analysis of RNAseq data, and Dr Amro Hamdoun for providing advice on live cell imaging.

Author contributions

DPY, MH and MT designed research; DPY performed the research; DPY, MH and MT analyzed data and interpreted the results; and DPY, MH and MT wrote the manuscript. MH and MT contributed equally to this work.

ORCID

Martin Tresguerres https://orcid.org/0000-0002-7090-9266
Daniel P. Yee https://orcid.org/0000-0002-2085-5538

References

Abbriano BR. 2017. *Insights into the molecular regulation of growth and carbon flux in marine diatoms*, PhD thesis. San Diego, La Jolla, CA, USA: University of California.

Bowman BJ, Bowman EJ. 2002. Mutations in subunit c of the vacuolar ATPase confer resistance to bafilomycin and identify a conserved antibiotic binding site. *Journal of Biological Chemistry* **277**: 3965–3972.

Bussard A, Lopez PJ. 2014. Evolution of vacuolar pyrophosphatases and vacuolar H^+-ATPases in diatoms. *Journal of Marine Science and Technology* **22**: 50–59.

Dames P, Zimmermann B, Schmidt R, Rein J, Voss M, Schewe B, Walz B, Baumann O. 2006. cAMP regulates plasma membrane vacuolar-type H^+-ATPase assembly and activity in blowfly salivary glands. *Proceedings of the National Academy of Sciences, USA* **103**: 3926–3931.

Darley WM, Volcani BE. 1969. Role of silicon in diatom metabolism: a silicon requirement for deoxyribonucleic acid synthesis in the diatom *Cylindrotheca fusiformis* Reimann and Lewin. *Experimental Cell and Research* **58**: 334–342.

Dröse S, Altendorf K. 1997. Bafilomycins and concanamycins as inhibitors of V-ATPases and P-ATPases. *Journal of Experimental Biology* **8**: 1–8.

Drum RW, Pankratz HS. 1964. Post mitotic fine structure of *Gomphonema parvulum*. *Journal of Ultrastructure Research* **10**: 217–223.

Falkowski PG, Barber RT, Smetacek V. 1998. Biogeochemical controls and feedbacks on ocean primary production. *Science* **281**: 200–207.

Falkowski PG, Grzebyk D, Katz ME, Knoll AH, Quigg A, Raven JA, Schofield O, Taylor FJR. 2004. The evolution of modern eukaryotic phytoplankton. *Science* **305**: 354–360.

Field CB, Behrenfeld MJ, Randerson JT, Falkowski PG. 1998. Primary production of the biosphere: Integrating terrestrial and oceanic components. *Science* **281**: 237–240.

Forgac M. 2007. Vacuolar ATPases: rotary proton pumps in physiology and pathophysiology. *Nature Reviews Molecular Cell Biology* **8**: 917–929.

Gordon R, Drum RW. 1994. The chemical basis of diatom morphogenesis. *International Review of Cytology* **150**: 243–372.

Görlich S, Pawolski D, Zlotnikov I, Kröger N. 2019. Control of biosilica morphology and mechanical performance by the conserved diatom gene *Silicanin-1*. *Communications Biology* **2**: 1–8.

Herve V, Derr J, Quinet M, Moisan L, Lopez PJ. 2012. Multiparametric analyses reveal the pH-dependence of silicon biomineralization in diatoms. *PLoS ONE* **7**: e46722.

Hildebrand M. 2010. 3D imaging of diatoms with ion-abrasion electron microscopy. *Journal of Structural Biology* **166**: 316–328.

Hildebrand M, Frigeri LG, Davis AK. 2007. Synchronized growth of *Thalassiosira Pseudonana (Bacillariophyceae)* provides novel insights into cell-wall synthesis processes in relation to the cell cycle. *Journal of Phycology* **740**: 730–740.

Hildebrand M, Lerch SJL, Shrestha RP. 2018. Understanding diatom cell wall silicification—moving forward. *Frontiers in Marine Science* **5**: 1–19.

Huss M, Ingenhorst G, Ko S, Gaßel M, Dro S, Zeeck A, Altendorf K, Wieczorek H. 2002. Concanamycin A, the specific inhibitor of V-ATPases, binds to the V_o subunit c. *Journal of Biological Chemistry* **277**: 40544–40548.

Iler RK. 1979. *The chemistry of silica: solubility, polymerization, colloid and surface properties, and biochemistry*. New York, USA: Wiley-Interscience.

Kawasaki-Nishi S, Nishi T, Forgac M. 2003. Proton translocation driven by ATP hydrolysis in V-ATPases. *FEBS Letters* **545**: 76–85.

Kluge C, Lahr J, Hanitzsch M, Bolte S, Golldack D, Dietz K. 2003. New insight into the structure and regulation of the plant vacuolar H^+-ATPase. *Journal of Bioenergetics and Biomembranes* **35**: 377–388.

© 2019 The Authors
New Phytologist © 2019 New Phytologist Trust

Kotzsch A, Gröger P, Pawolski D, Bomans PHH, Sommerdijk NAJM, Schlierf M, Kröger N. 2017. Silicanin-1 is a conserved diatom membrane protein involved in silica biomineralization. *BMC Biology* **15**: 65.

Kotzsch A, Pawolski D, Milentyev A, Shevchenko A, Scheffel A, Poulsen N, Shevchenko A, Kröger N. 2016. Biochemical composition and assembly of biosilica-associated insoluble organic matrices from the diatom *Thalassiosira pseudonana*. *Journal of Biological Chemistry* **291**: 4982–4997.

Kröger N, Deutzmann R, Bergsdorf C, Sumper M. 2000. Species-specific polyamines from diatoms control silica morphology. *Proceedings of the National Academy of Sciences, USA* **97**: 14133–14138.

Kröger N, Deutzmann R, Sumper M. 1999. Polycationic peptides from diatom biosilica that direct silica nanosphere formation. *Science* **286**: 1129–1132.

Kröger N, Lorenz S, Brunner E, Sumper M. 2002. Self-assembly of highly phosphorylated silaffins and their function in biosilica morphogenesis. *Science* **298**: 584–586.

Maxson ME, Grinstein S. 2014. The vacuolar-type H^+-ATPase at a glance - more than a proton pump. *Journal of Cell Science* **127**: 4987–4993.

Milligan AJ, Morel FMM. 2002. A proton buffering role for silica in diatoms. *Science* **297**: 1848–1850.

Nishi T, Forgac M. 2002. The vacuolar (H^+)-ATPases — nature's most versatile proton pumps. *Nature Reviews Molecular Cell Biology* **3**: 94–103.

Pastor-Soler N, Beaulieu V, Litvin TN, Da Silva N, Chen Y, Brown D, Buck J, Levin LR, Breton S. 2003. Bicarbonate-regulated adenylyl cyclase (sAC) is a sensor that regulates pH-dependent V-ATPase recycling. *Journal of Biological Chemistry* **278**: 49523–49529.

Pickett-Heaps JD, Schmid AMM, Edgar LA.1990. The cell biology of diatom valve formation. In: Round FE, Chapman DJ, eds. *Progress in phycological research*. Bristol, UK: Biopress Ltd, 1–168.

Poulsen N, Chesley PM, Kröger N. 2006. Molecular genetic manipulation of the diatom *Thalassiosira pseudonana (Bacillariophyceae)*. *Journal of Phycology* **42**: 1059–1065.

Poulsen N, Kröger N. 2004. Silica morphogenesis by alternative processing of silaffins in the diatom *Thalassiosira pseudonana*. *Journal of Biological Chemistry* **279**: 42993–42999.

Raven JA. 1983. The transport and function of silicon in plants. *Biological Reviews* **58**: 179–207.

Roa JN, Tresguerres M. 2016. Soluble adenylyl cyclase is an acid-base sensor in epithelial base-secreting cells. *American Journal of Physiology – Cell Physiology* **311**: C340–C349.

Romero-Calvo I, Ocón B, Martínez-Moya P, Suárez MD, Zarzuelo A, Martínez-Augustin O, de Medina FS. 2010. Reversible Ponceau staining as a loading control alternative to actin in Western blots. *Analytical Biochemistry* **401**: 318–320.

Roy JW, Hill E, Ruan YC, Vedovelli L, Paunescu TG, Brown D, Breton S. 2013. Circulating aldosterone induces the apical accumulation of the proton pumping V-ATPase and increases proton secretion in clear cells in the caput epididymis. *American Journal of Physiology – Cell Physiology* **305**: C436–C446.

Schindelin J, Arganda-carreras I, Frise E, Kaynig V, Longair M, Pietzsch T, Preibisch S, Rueden C, Saalfeld S, Schmid B *et al.* 2019. Fiji: an open-source platform for biological-image analysis. *Nature Methods* **9**: 676–682.

Schmid AMM, Schulz D. 1979. Wall morphogenesis in diatoms: Deposition of silica by cytoplasmic vesicles. *Protoplasma* **100**: 267–288.

Shimizu K, Del Amo Y, Brzezinski MA, Stucky GD, Morse DE. 2001. A novel fluorescent silica tracer for biological silicification studies. *Chemistry and Biology* **8**: 1051–1060.

Sumper M, Kröger N. 2004. Silica formation in diatoms: the function of long-chain polyamines and silaffins. *Journal of Materials Chemistry* **14**: 2059–2065.

Sze H, Schumacher K, Müller ML, Padmanaban S, Taiz L. 2002. A simple nomenclature for a complex proton pump: VHA genes encode the vacuolar H^+-ATPase. *Trends in Plant Science* **7**: 157–161.

Sze H, Ward JM, Lai S. 1992. Vacuolar H+-translocating ATPases from plants: Structure, function, and isoforms. *Journal of Bioenergetics and Biomembranes* **24**: 371–381.

Tesson B, Hildebrand M. 2013. Characterization and localization of insoluble organic matrices associated with diatom cell walls: Insight into their roles during cell wall formation. *PLoS ONE* **8**: e61675.

Tesson B, Lerch SJL, Hildebrand M. 2017. Characterization of a new protein family associated with the silica deposition vesicle membrane enables genetic manipulation of diatom silica. *Scientific Reports* **7**: 1–13.

Tresguerres M. 2016. Novel and potential physiological roles of vacuolar-type H^+-ATPase in marine organisms. *Journal of Experimental Biology* **219**: 2088–2097.

Tresguerres M, Parks SK, Salazar E, Levin LR, Goss GG, Buck J. 2010. Bicarbonate-sensing soluble adenylyl cyclase is an essential sensor for acid/base homeostasis. *Proceedings of the National Academy of Sciences, USA* **107**: 442–447.

Vartanian M, Desclés J, Quinet M, Douady S, Lopez PJ. 2009. Plasticity and robustness of pattern formation in the model diatom *Phaeodactylum tricornutum*. *New Phytologist* **182**: 429–442.

Volcani BE, Li CW. 1984. Aspects of silicification in wall morphogenesis of diatoms. *Philosophical Transactions of the Royal Society B: Biological Sciences* **304**: 519–528.

Vrieling EG, Gieskes WWC, Beelen TPM. 1999. Silicon deposition in diatoms: Control by the pH inside the silicon deposition vesicle. *Journal of Phycology* **35**: 548–559.

Xiao Y-T, Xiang L-X, Shao J-Z. 2008. Vacuolar H^+-ATPase. *International Journal of Biochemistry and Cell Biology* **40**: 2002–2006.

Yool A, Tyrrell T. 2003. Role of diatoms in regulating the ocean's silicon cycle. *Global Biogeochemical Cycles* **17**: 1–21.

Supporting Information

Additional Supporting Information may be found online in the Supporting Information section at the end of the article.

Fig. S1 Representative images of exponentially growing *T. pseudonana* natively expressing VHA_B-eGFP.

Fig. S2 Western blots of VHA_B protein abundance in *T. pseudonana* cultures throughout the cell cycle along with corresponding Ponceau-stained blots.

Fig. S3 Representative images of cell cycle-synchronized *T. pseudonana* expressing fcp-VHA_B-eGFP incubated with 5 nM concanamycin A.

Fig. S4 Representative images of cell cycle-synchronized *T. pseudonana* expressing fcp-SAP1-eGFP –/+ 5 nM concanamycin A.

Fig. S5 Suboptimal VHA activity results in altered valve nanostructure, examined by SEM after 22 h growth in 0.4 nM concanamycin A conditions.

Video S1 Time-lapse imaging video of *T. pseudonana* expressing fcp-VHA_B-eGFP during valve biosynthesis (MP4 803 kb).

Video S2 Time-lapse imaging video of *T. pseudonana* expressing fcp-VHA_B-eGFP during girdle band biosynthesis (MP4 888 kb).

Please note: Wiley Blackwell are not responsible for the content or functionality of any Supporting Information supplied by the authors. Any queries (other than missing material) should be directed to the *New Phytologist* Central Office.

© 2019 The Authors
New Phytologist © 2019 New Phytologist Trust

New Phytologist Supporting Information

Article title: Dynamic subcellular translocation of V-type H^+-ATPase is essential for biomineralization of the diatom silica cell wall

Authors: Daniel P. Yee, Mark Hildebrand, Martin Tresguerres

Article acceptance date: 4 November 2019

The following supporting information is available for this article:

Fig. S1 VHA localization in multiple subcellular compartments. Representative images of exponentially growing *T. pseudonana* natively expressing VHA_B-eGFP in **(a)** vacuole tonoplast and cytosol, **(b)** valve SDV and vacuole tonoplast, and **(c)** vacuole tonoplast and cytosol post cell division. Green: VHA_B-eGFP; red: chlorophyll; differential interference contrast. Scale bar: 5 µm.

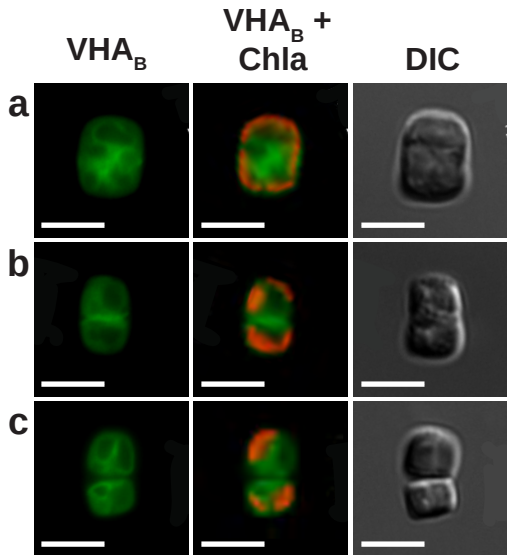


Fig. S2 VHA_B protein abundance in *T. pseudonana* cultures throughout the cell cycle. VHA_B protein abundance was quantified by Western blotting using a monoclonal VHA_B antibody in *T. pseudonana* cultures expressing fcp-VHA_B-eGFP at the indicated times following silicon re-addition. **(a-e)** Western blots of replicate cultures. The ~56 KDa band corresponds to native VHA_B; the ~89 KDa band corresponds to VHA_B-eGFP. **(f-j)** Ponceau stained blots confirmed equivalent total protein loaded per lane for each corresponding blot.

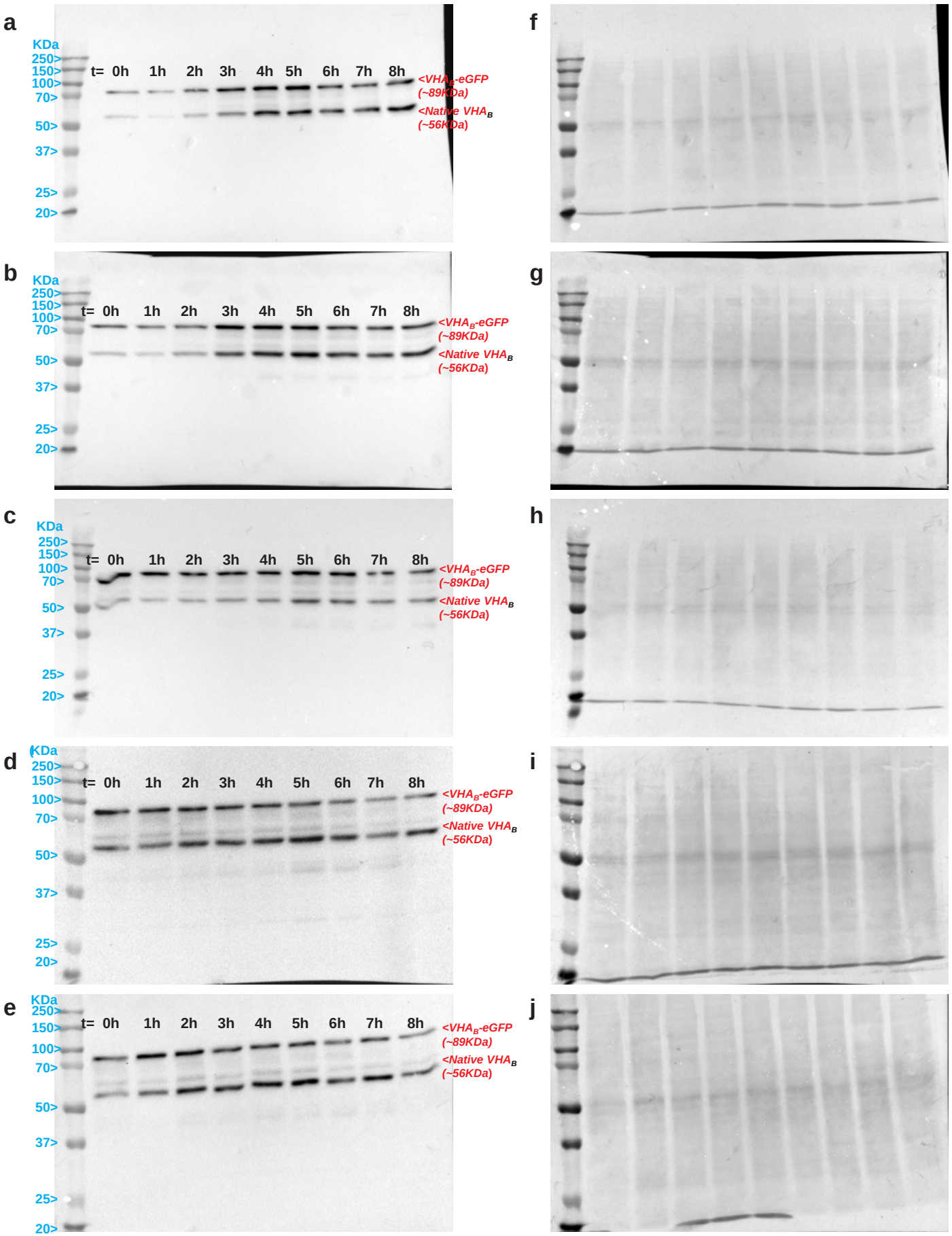
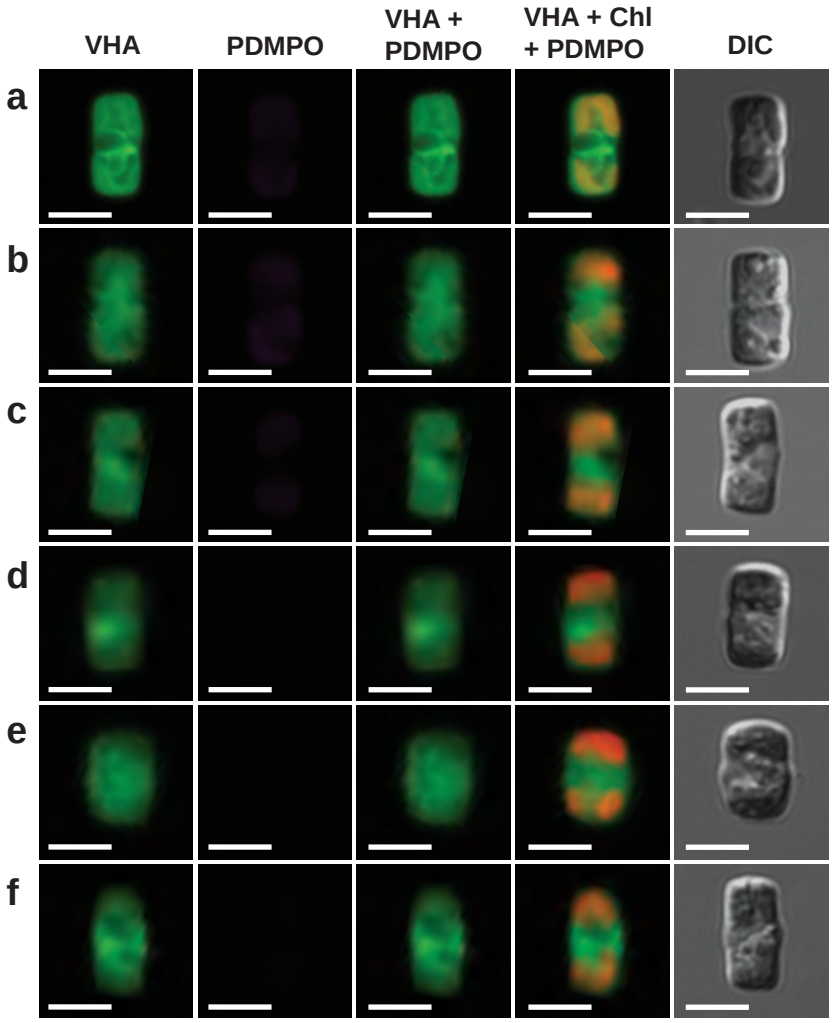


Fig. S3 Inhibition of VHA activity prevents SDV acidification and frustule formation (this figure expands on **Fig. 5**). **(a-f)** Representative images of cell cycle synchronized *T. pseudonana* expressing fcp-VHA_B-eGFP incubated with 5 nM concanamycin A. Green: VHA_B-eGFP; magenta: PDMPO; white: colocalization of VHA_B-eGFP and PDMPO; red: chlorophyll; differential interference contrast. Scale bar: 5 µm.



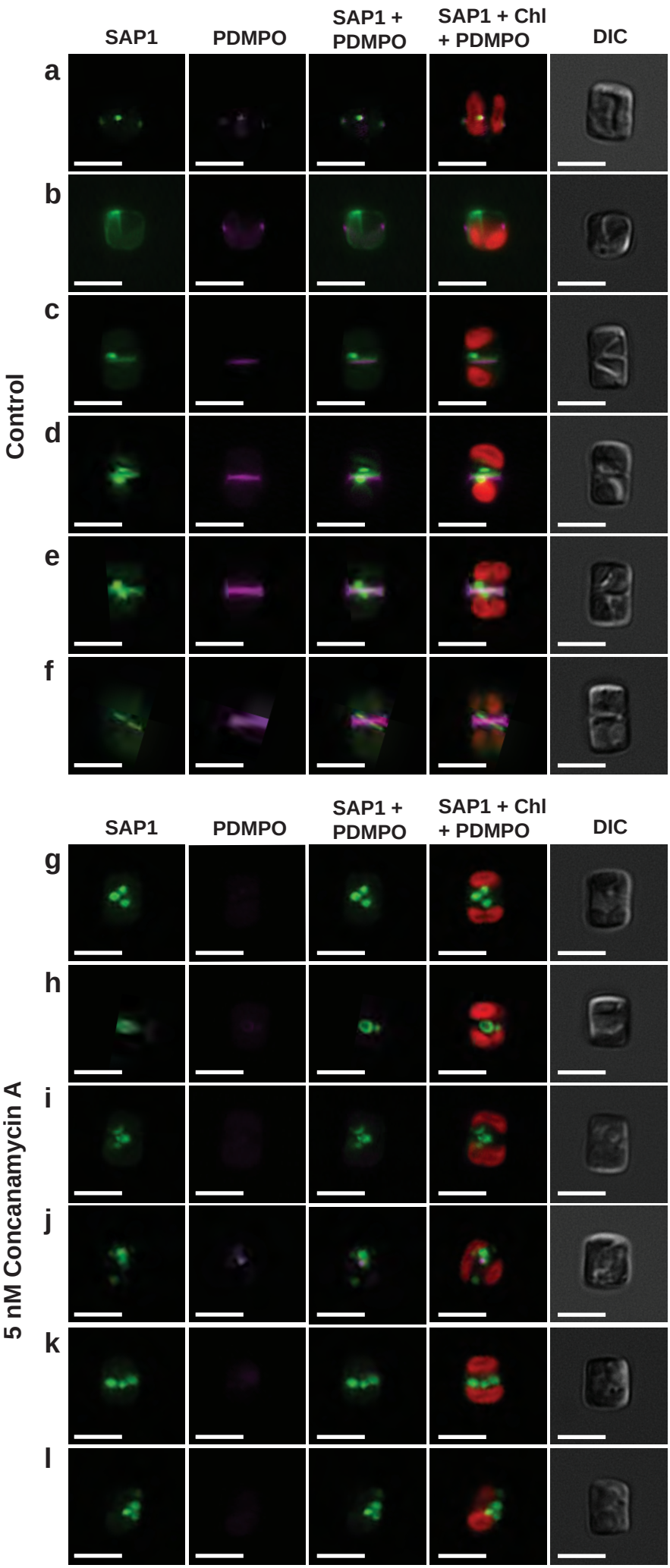
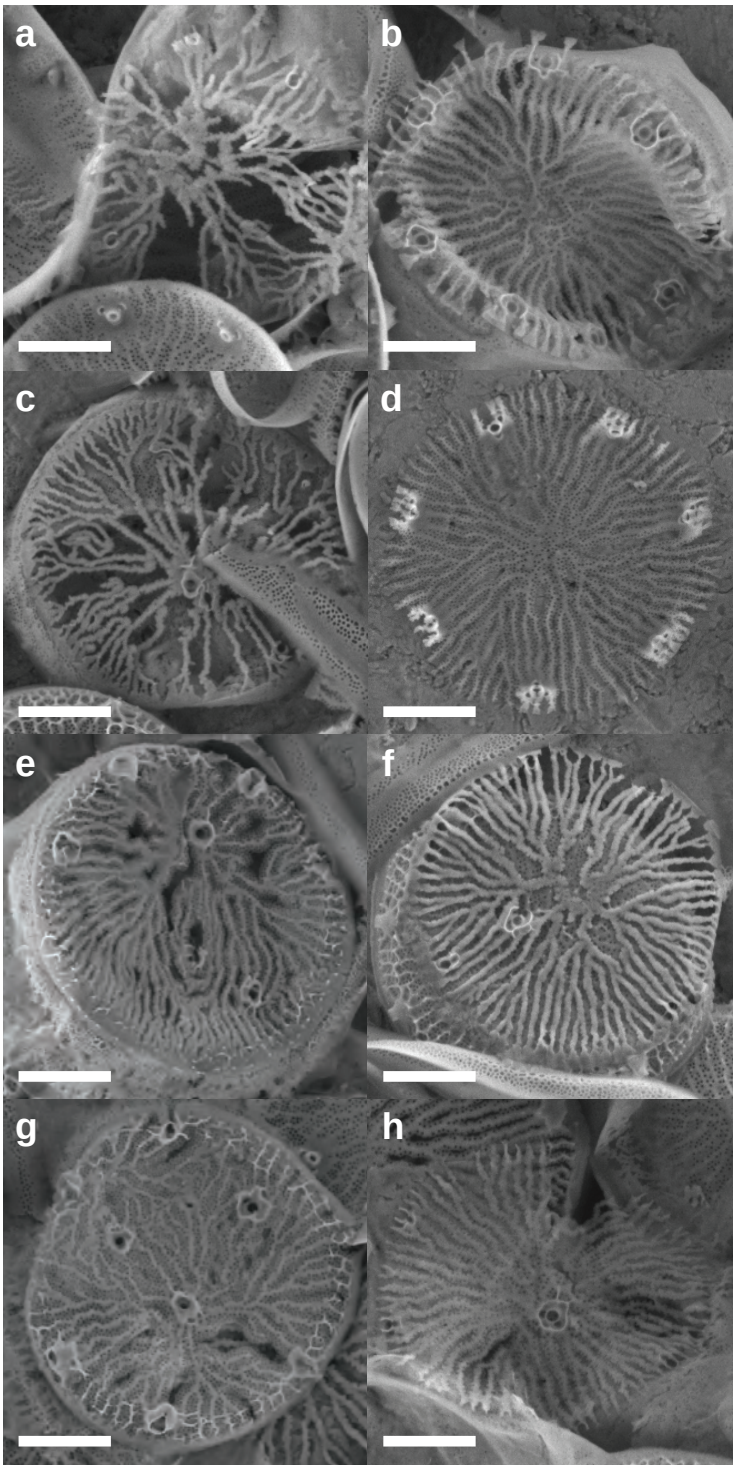


Fig. S4 Inhibition of VHA activity prevents insertion of SAP1 into the SDV (this figure expands on **Fig. 8**). Representative images of cell cycle synchronized *T. pseudonana* expressing fcp-SAP1-eGFP. **(a-f)** Control cells. **(g-l)** Cells incubated with 5 nM concanamycin A. Green: SAP1-eGFP; magenta: PDMPO; white: colocalization of SAP1-eGFP and PDMPO; red: chlorophyll; differential interference contrast. Scale bar: 5 µm.

Fig. S5 (a-h) Suboptimal VHA activity results in a range of altered valve nanostructure, examined by SEM after 22h incubation with 0.4 nM concanamycin A conditions (this figure expands on **Fig. 9**). Scale bars: 1 µm.



Video S1 Time-lapse imaging video of *T. pseudonana* expressing fcp-VHA_B-eGFP during valve biosynthesis [MP4 803 kb] (see separate file)

Video S2 Time-lapse imaging video of *T. pseudonana* expressing fcp-VHA_B-eGFP during girdle band biosynthesis [MP4 888 kb](see separate file)